Electronic Supplementary Material (ESI) for Energy & Environmental Science.

Supporting Information

Sustainable High Voltage Source based on Triboelectric Nanogenerator with charge accumulation strategy

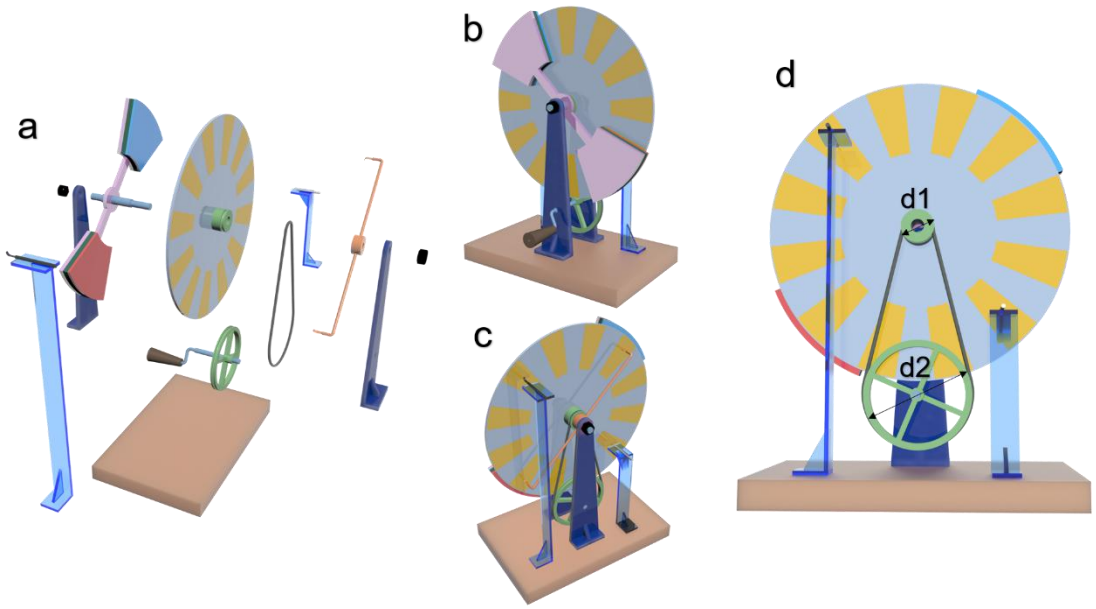

Supplementary Figure S1. Equal scale model of SH-TNEG. a) Exploded Views of whole SH-TENG. b, c) Axonometric view of whole SH-TENG. d) Speed-increasing mechanism, d2=4d1.

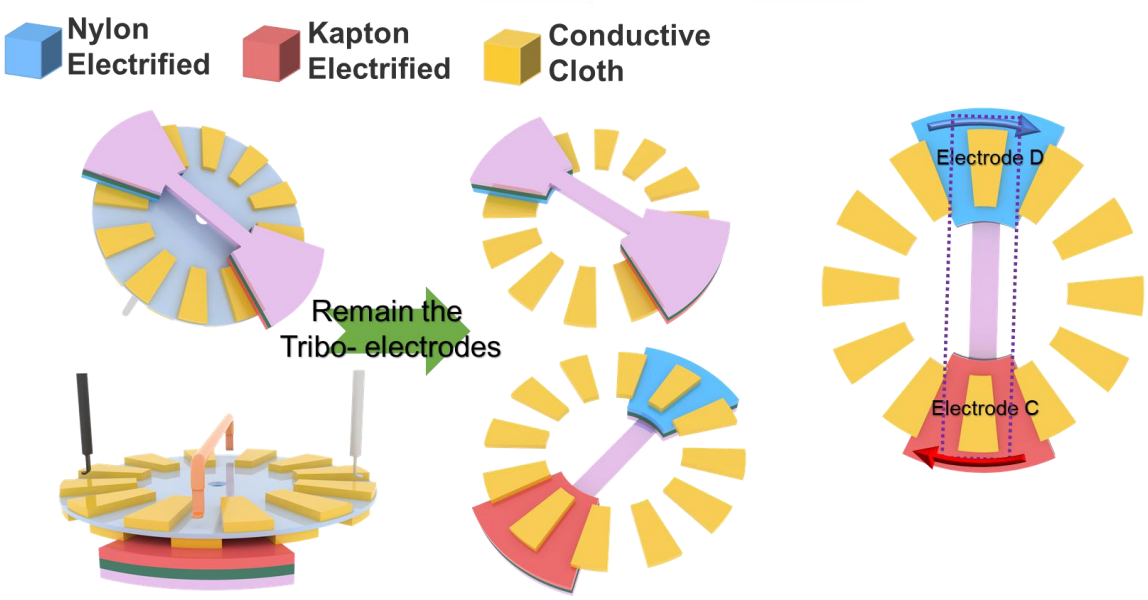

Supplementary Figure S2. Hide irrelevant parts to explain the process of tribo-electrification

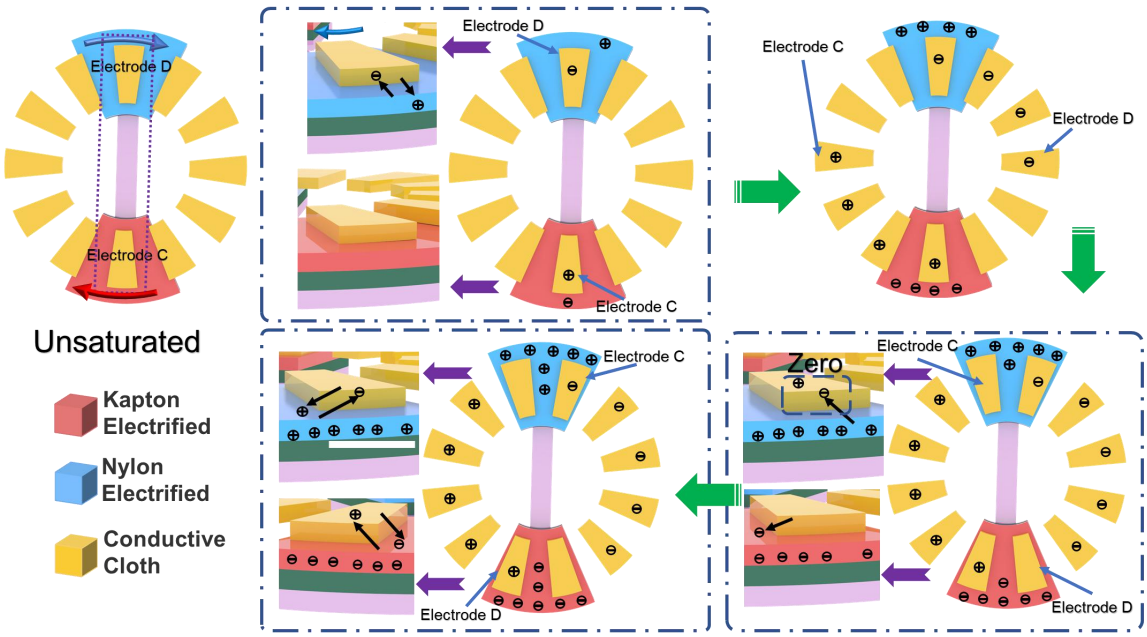

Supplementary Figure S3. Charge transfer between tribo-electrodes and dielectric layers when the dielectric layers does not reach charge saturation state

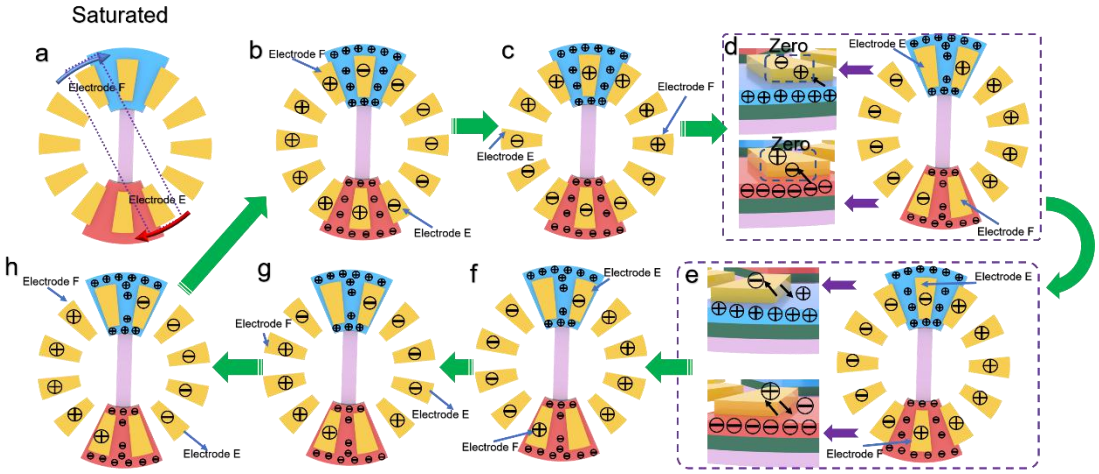

Supplementary Figure S4. Charge transfer between tribo-electrodes and dielectric layers when the dielectric layers reach charge saturation state

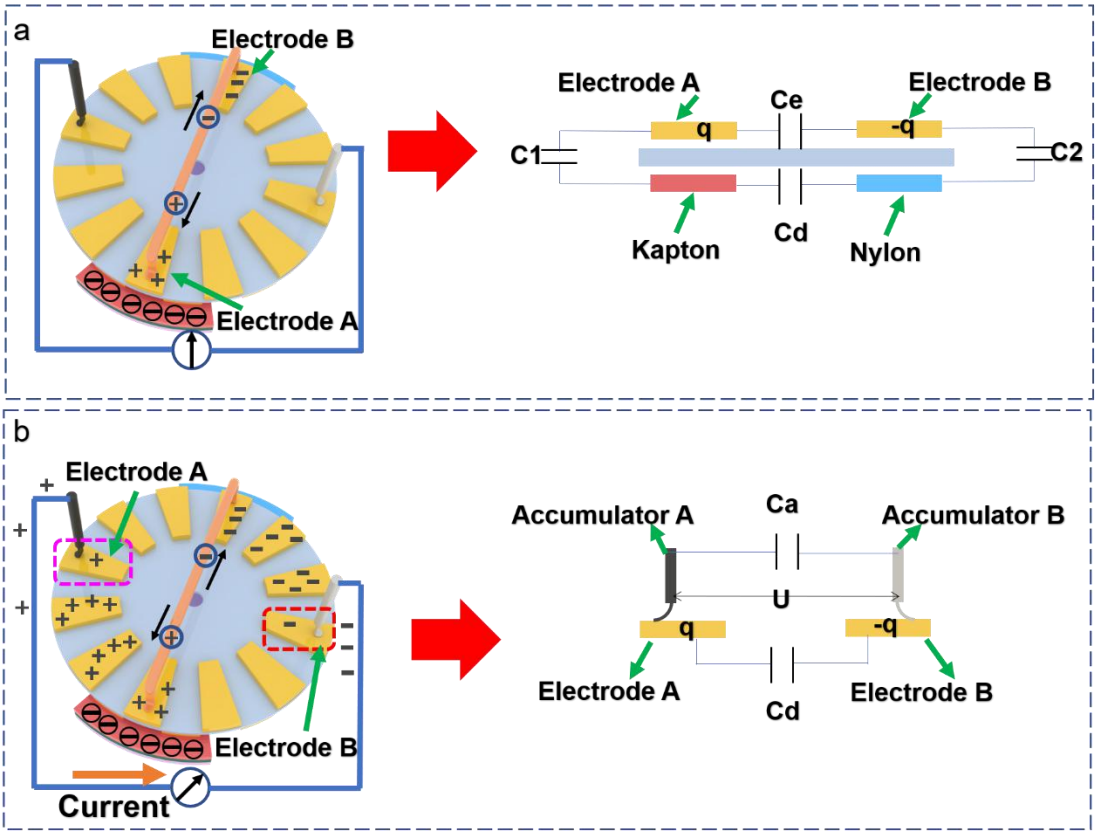

Supplementary Figure S5. Physical model of SH-TNEG. a) Equivalent physical model of electrostatic induction process. b) Equivalent physical model of charge accumulation process.

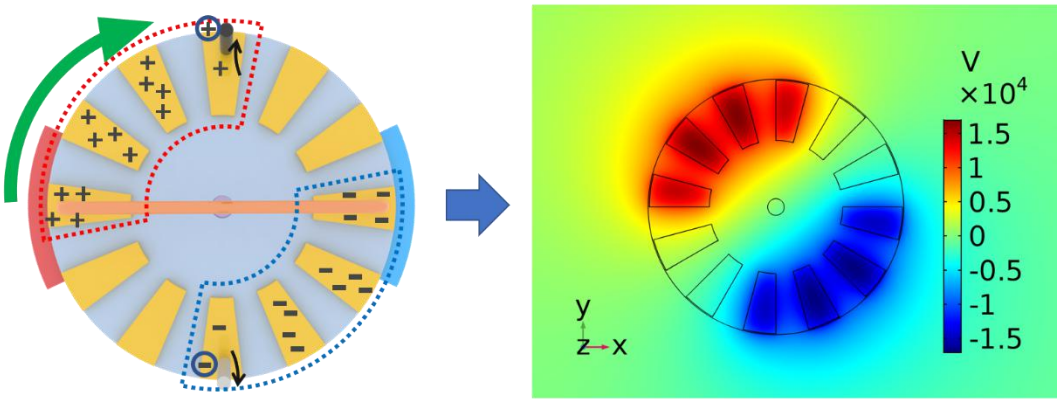

Supplementary Figure S6. Potential simulation via COMSOL between the transporting-electrodes when disk rotates.

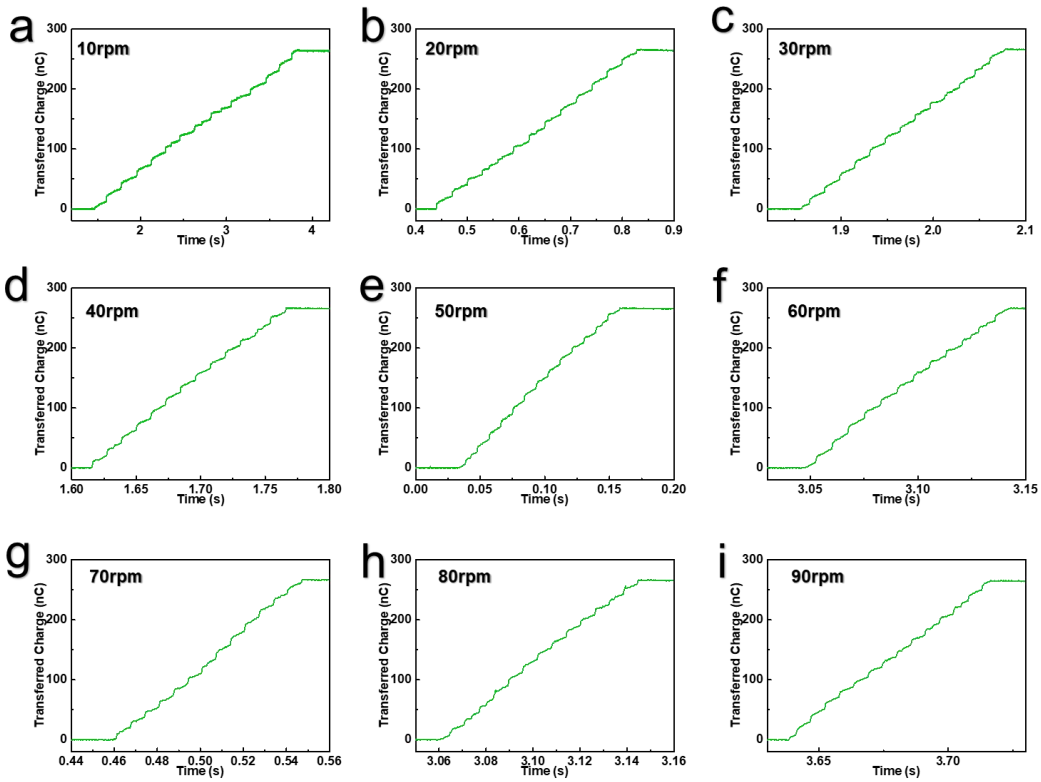

Supplementary Figure S7. Transferred Charge of SH-TENG with different rotation speed, the central angle is fixed at 15°.

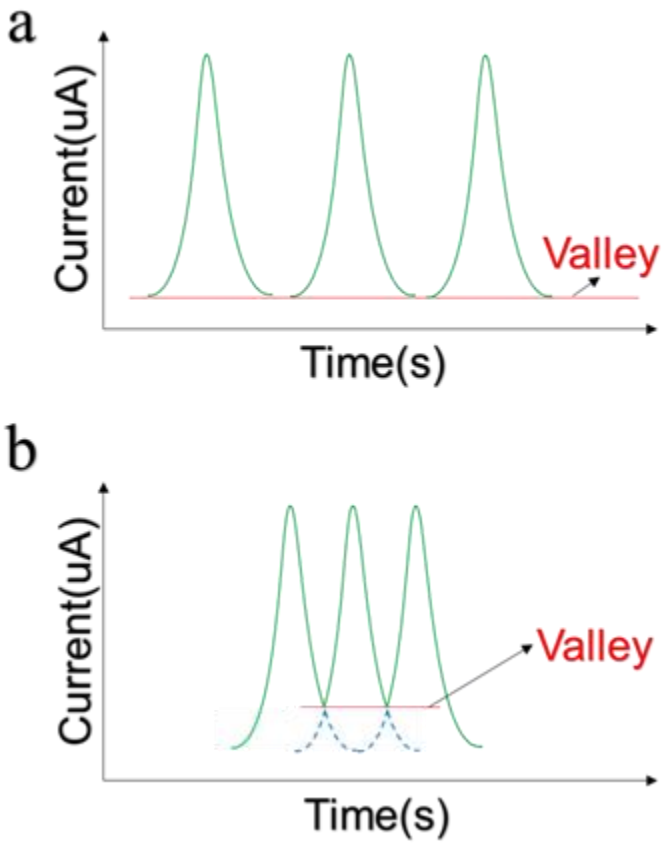

Supplementary Figure S8. Schematic diagram of each signal with (a)low frequency;(b)high frequency.

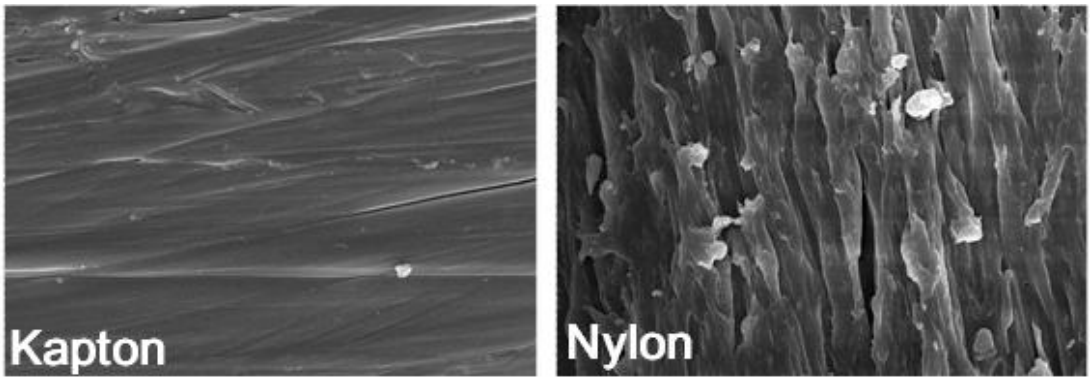

Supplementary Figure S9. The SEM images of Kapton and Nylon after 10 thousands cycles of friction, respectively.

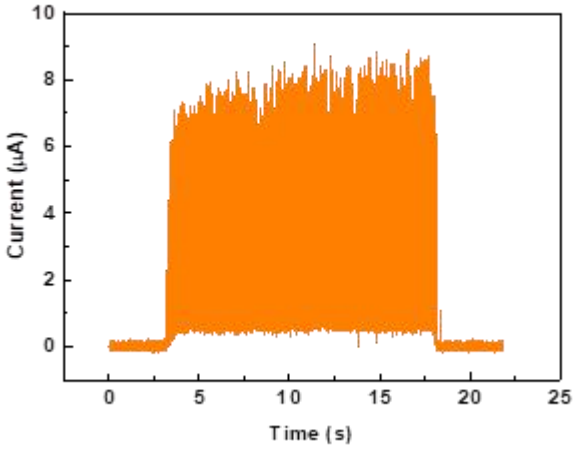

Supplementary Figure S10. The short-circuit current (Isc) of TENG after 10 thousands motion cycles.

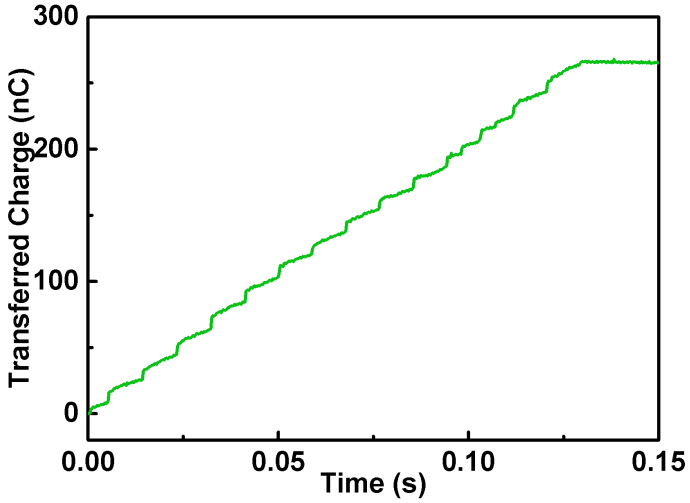

Supplementary Figure S11. The transferred charge (Qsc) of TENG after 10 thousands motion cycles.

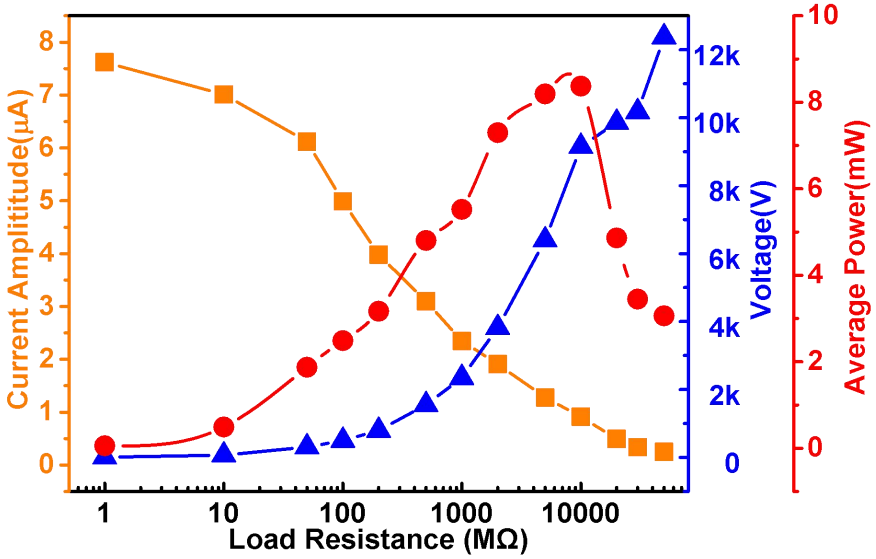

Supplementary Figure S12. The voltage/current vs. load curves of TENG after thousands cycles of friction.

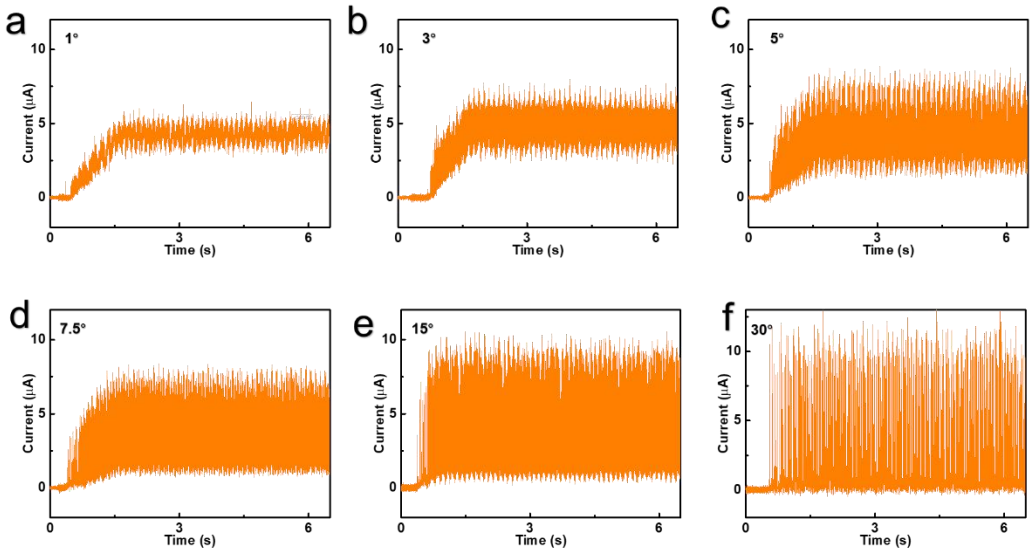

Supplementary Figure S13. Short-Circuit Current of SH-TENG with different central angle at 50rpm.

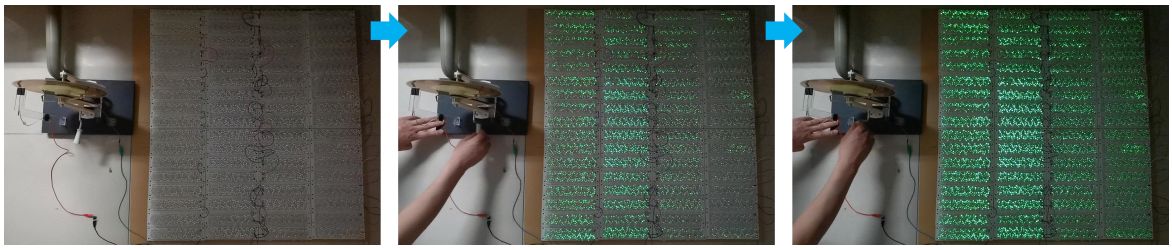

Supplementary Figure S14 more than 8000 LEDs are lighted up by SH-TENG with central angle of electrode at 1°.

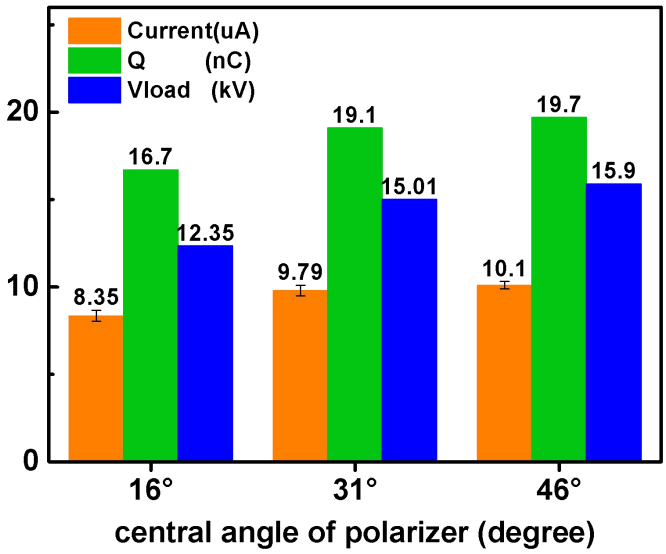

Supplementary Figure S15. The output performance of the SH-TENG with different central angle of polarizer

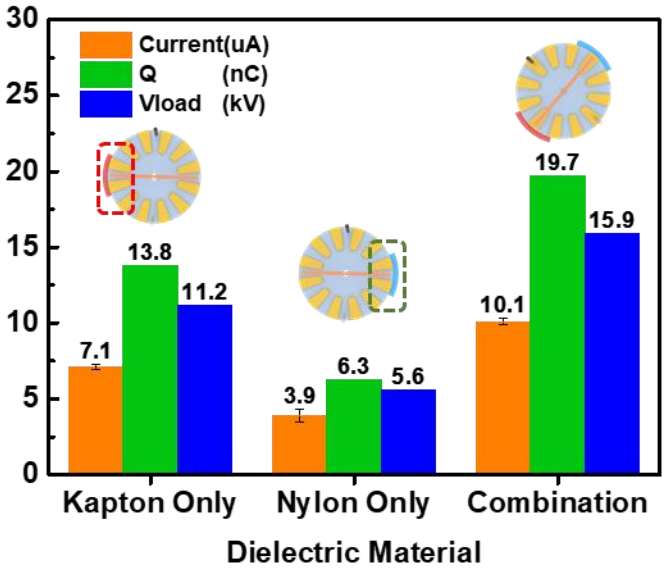

Supplementary Figure S16. The output performance of the SH-TENG when different dielectric material is remained.

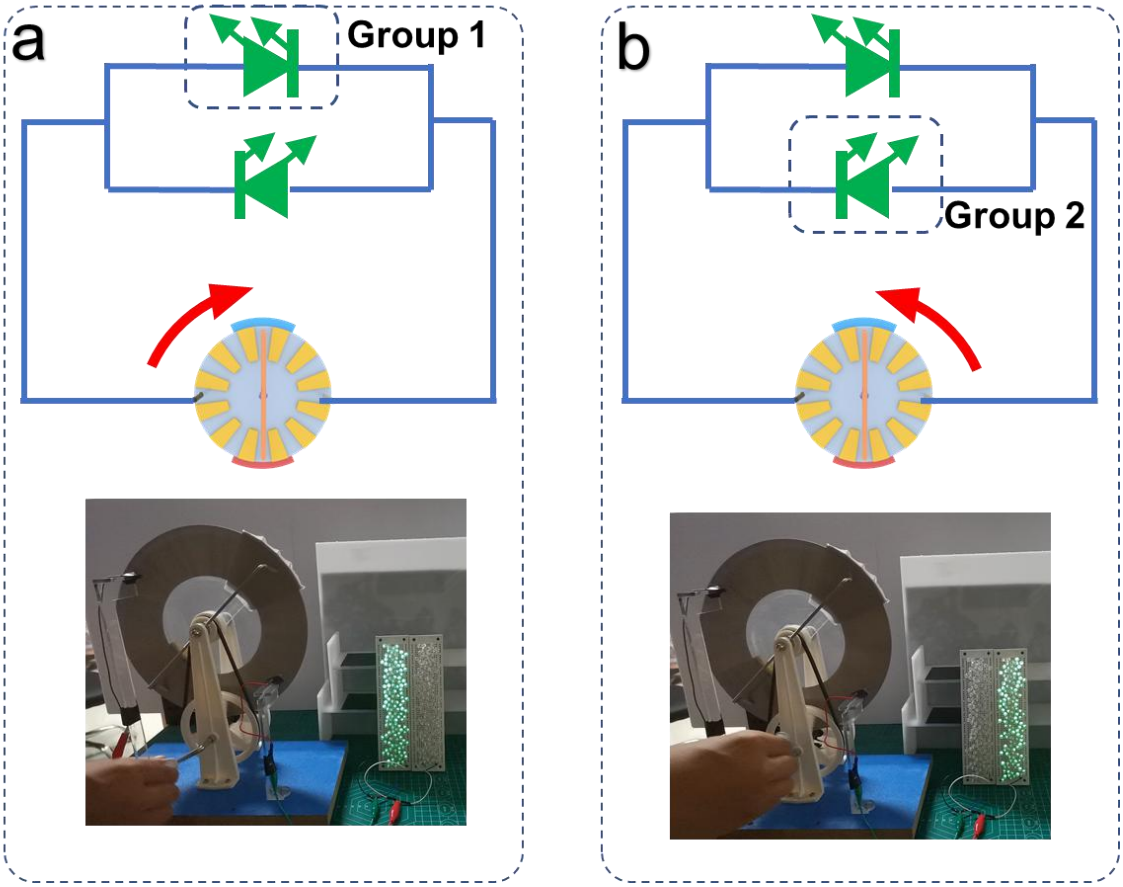

Supplementary Figure S17. Demonstrations of the SH-TENG to light up 120 LEDs with different rotational direction.

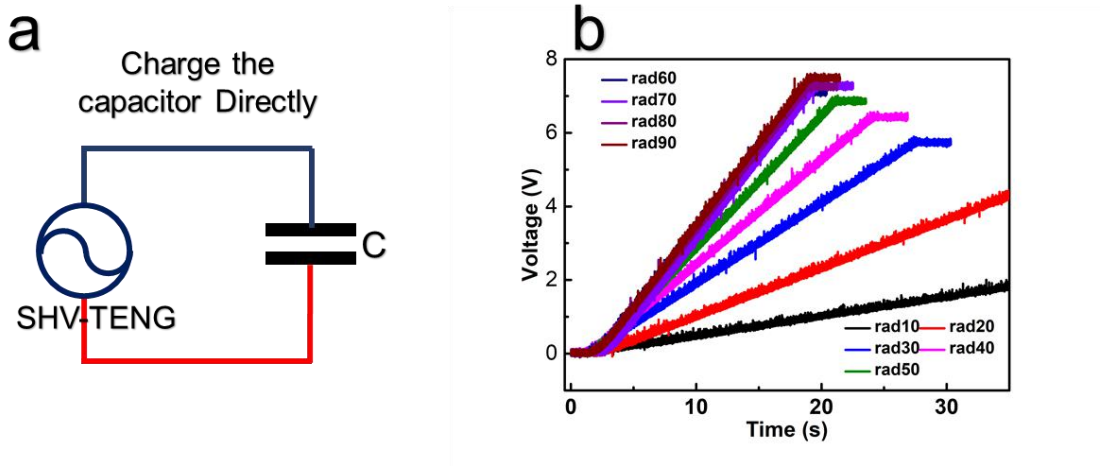

Supplementary Figure S18. Influence on the change of rotation speed when charging a 10uF capacitor.

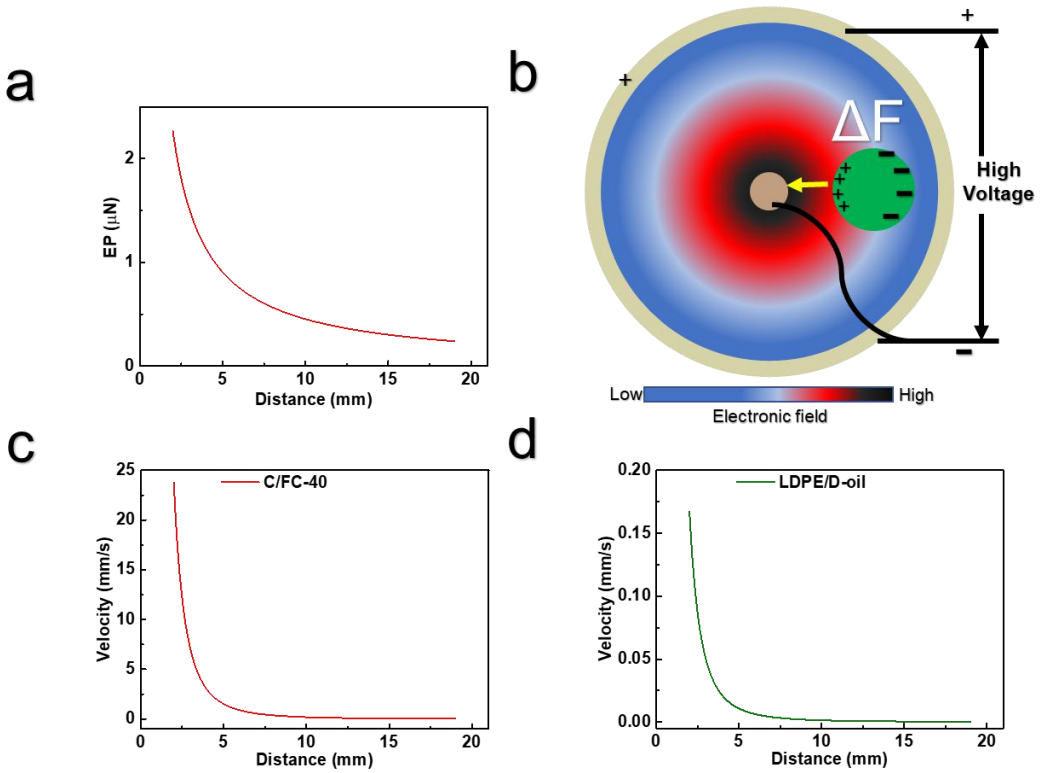

Supplementary Figure S19. a) Electrophoretic force at different positions from the central electrode. b) The schematic diagram of dielectrophoresis force. c, d) Velocity of single particle of LDPE and C in corresponding solution when particles only affected by dielectrophoresis force.

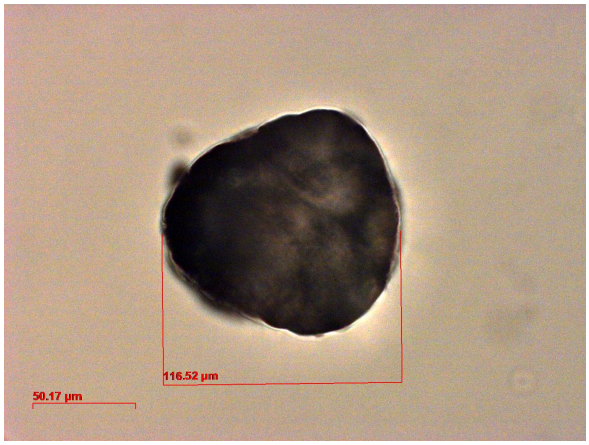

Supplementary Figure S20. The morphology of particle (LDPE)

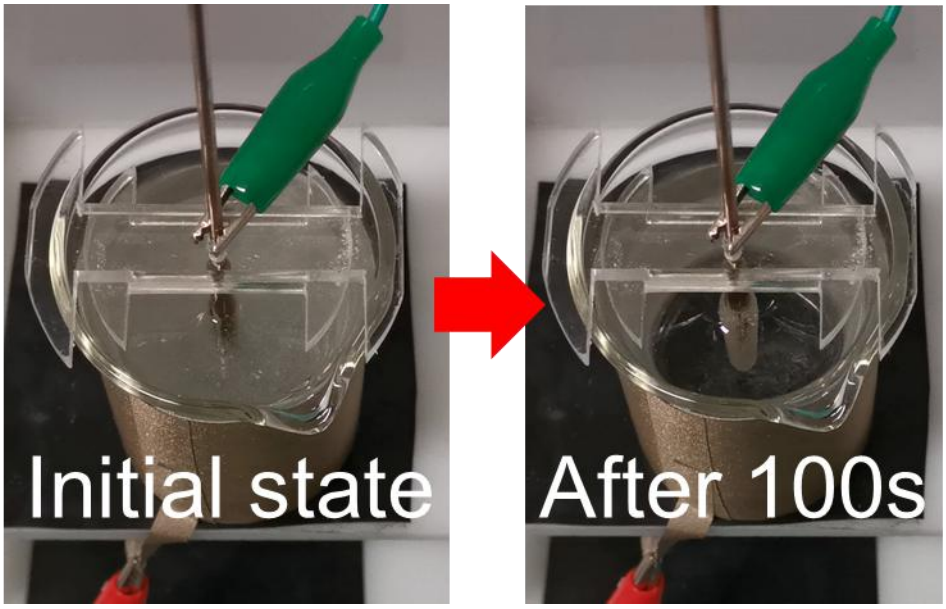

Supplementary Figure S21. Photograph of SH-TENG to purify the dispersed LDPE in the dimethylsilicone oil within 100s with reverse rotation.

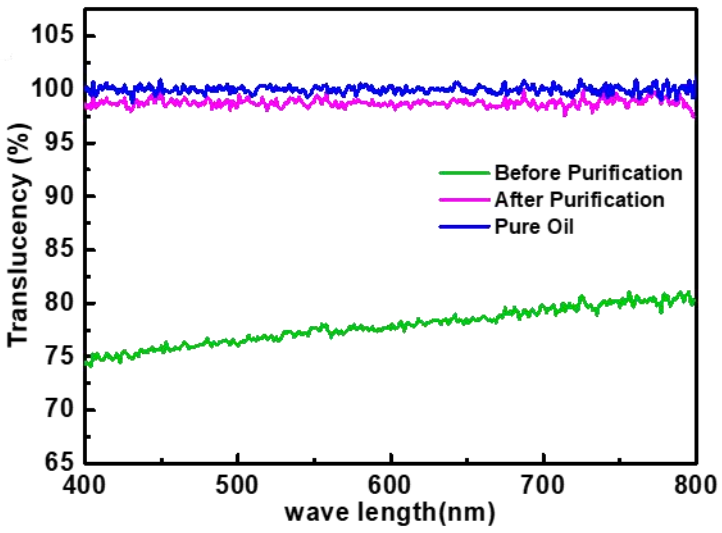

Supplementary Figure S22. Translucency of LDPE in dimethlsilicone oil before and after purification (purification time: 100 seconds);

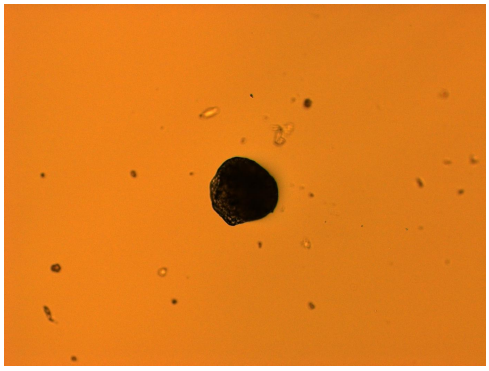

Supplementary Figure S23. The morphology of particles (LDPE) in 10uL oil

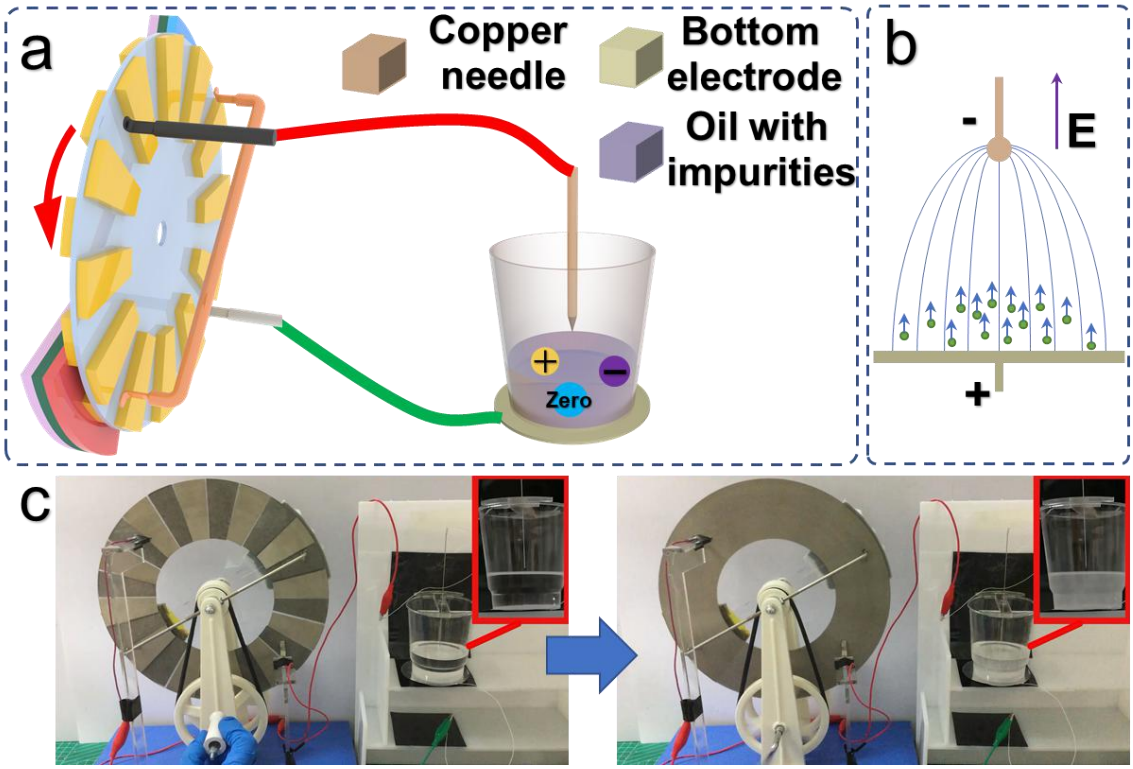

Supplementary Figure S24. Oil agitation system and its practical effect demonstration. a) Schematic diagram of oil agitation system. b) The electric field distribution profile inside the space. c) Photograph of SH-TENG to stir the precipitated LDPE evenly into dimethylsilicone oil within 10s.

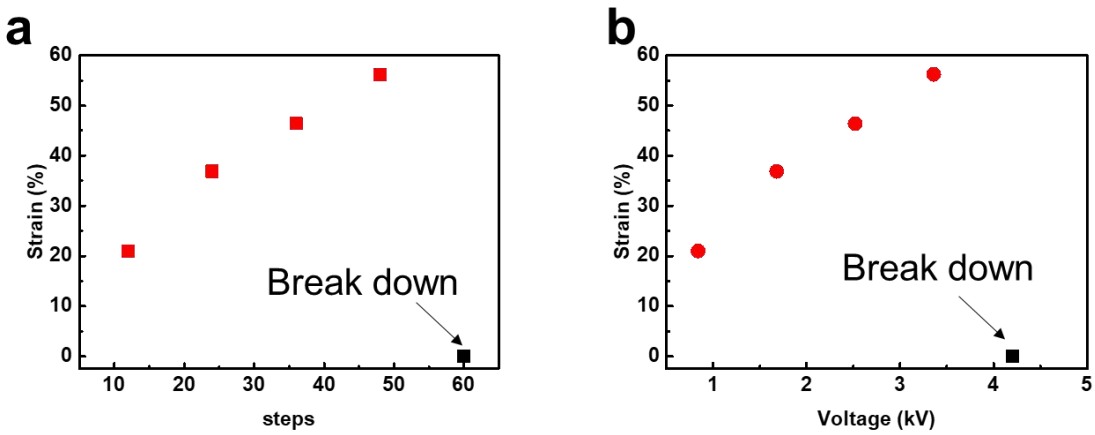

Supplementary Figure S25.a) The dependence of actuated strain with different moving steps from initial state of DEA. The deformation strain is defined as the ratio between the area increase of DEA under activation and its original area. b) The dependence of actuated strain with the calculated applied voltage from initial state of DEA. The strain is calculated according to equation Strain = (A − A0)/A0 × 100%, where A is the actuated area of carbon electrode and A0 is the original area.

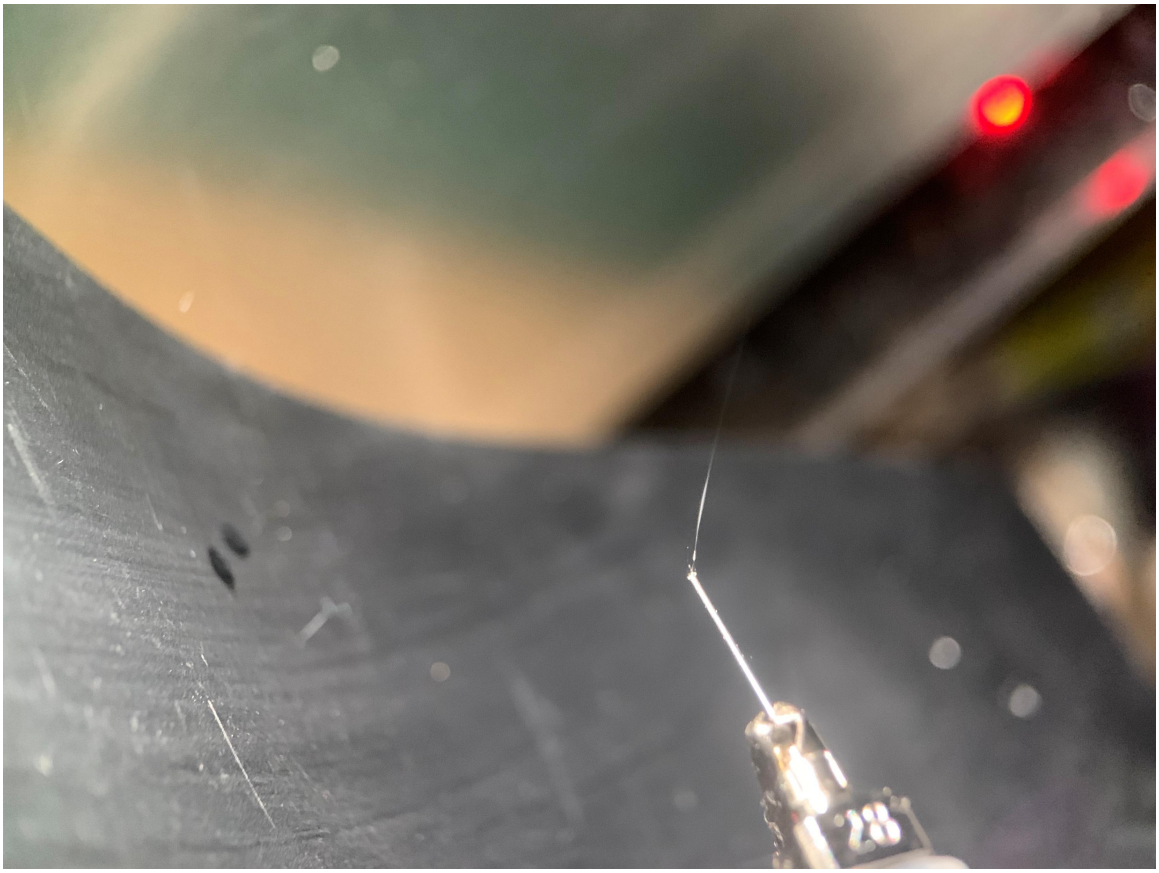

Supplementary Figure S26.The consecutive Taylor cone triggered by the rotation of SH-TENG

Supplementary Note S1: The detail process of triboelectrification between tribo-electrodes and dielectric materials.

To better demonstrate the process of triboelectrification between the tribo-electrodes and the dielectric layers, we only pick out the tribo-electrodes for discussion, as shown in Figure S1. Noting that the dielectric layers are not charged initially. Take the pair of tribo-electrodes (named electrode C and electrode D) as shown in Figure S1 for demonstration, when disk rotates clockwise, the pair of tribo-electrodes rubs against the dielectric layers. Due to triboelectrification, electrode C is positively charged while Kapton is negatively charged, and electrode D is negatively charged while Nylon is positively charged, as shown in Figure S2a. With the rotation of the disk, the pair of tribo-electrodes is away from the dielectric layers, and more tribo-charges are accumulated on the dielectric layers, as shown in Figure S2b. With the disk rotates half a circle, the positively charged electrode C rubs against Nylon while the negatively charged electrode D rubs against Kapton. According to the tendency to gain or lose electrons of various materials, Nylon loses electrons to electrode C while Kapton gains electrons from electrode D. Electrode C and electrode D are in a temporary charge neutralization state, as shown in Figure S2c. The temporary charge neutralization state is broken due to the continuously friction between the pair of tribo-electrodes and the dielectric layers, and once again Nylon loses electrons to electrode C to make a negatively charged state of electrode C, while Kapton gains electrons from electrode D to induce the electrode D positively charged, as shown in Figure S2d. With the continuous rotation of disk, the dielectric layers gradually come to the electrified saturation state.

When the dielectric layers come to the electrified saturation state, the phenomenon of triboelectrification between tribo-electrodes and dielectric layers still exists. Another pair of tribo-electrodes (electrode E and electrode F) is chosen to demonstrate the process. As shown in Figure S3b, the pair of tribo-electrodes is not contact with the dielectric layer, with the electrode E negatively charged while the electrode F positively charged. The charges on the pair of tribo-electrodes are maintained after the disk moves a quarter circle, as shown in Figure S3c. When the pair of tribo-electrodes fully contact with the dielectric layers, the electrode E and the electrode F are in charge neutralization state instantly as shown in Figure S3d, inducing a temporary charge-unsaturated state of the dielectric layers. But the dielectric layers become charge-saturated immediately due to the friction with electrode E and electrode F, as shown in Figure S3e. Subsequent electrodes continue to rub against the dielectric layers to repeat the similar procedure, as shown in Figure S3f, Figure S3g and Figure S3h. Thus, we can assume that the dielectric layers are in charge saturated state during the whole process.

Supplementary Note S2: Theoretical calculation of Q_A and $Q_{leakage}$.

(1) The calculation of charge amount on accumulators ($\mathbf{Q_A}$):

The time for the disk to rotate at a uniform rate per circle can be obtained as following equation:

$$T = \frac{2\pi}{\omega} \quad (1)$$

Where ω is the angular velocity of disk. When the disk rotates, the time interval between the single accumulator and the adjacent transporting-electrodes is obtained as

$$\triangle t = \frac{T}{\mathrm{N}} = \frac{2\pi}{\mathrm{N}\cdot\omega} \quad (2)$$

While the rotation speed of disk is

$$n = \frac{\omega}{2\pi} \cdot 60 \quad (3)$$

Combined equation (2) and (3), the amount of charges on accumulators is obtained as

$$Q_A = (\frac{t}{\triangle\ t}) \cdot q = \left[\frac{N \cdot \omega \cdot t}{2\pi}\right] \cdot q = (\left[\frac{Nnt}{60}\right])q \quad (4)$$

(2) The deduction of charge leakage on accumulators ($\mathbf{Q_{leakage}}$)

Define the leakage current as $i_{leakage}=dQ_{leakage}/dt$, and the density of the leakage current can be defined as $j_{leakage}=i_{leakage}/S_A$, where S_A is the exposure area of accumulators in air. The density of leakage current ($j_{leakage}$) can be related to the electric field (E) as $j_{leakage}=\sigma_o \exp(E/E_r)E$, where σ_o is the basic conductivity at low field and E_r is an empirical constant.[1, 2] In this case, the σ_o can be replaced as the basic conductivity of medium in contact with accumulators , and electric field E is relevant to the charge amount on accumulators ($\mathbf{Q_A}$). Similarly, the empirical constant E_r can be replaced as the new empirical constant Q_B which has the same dimension as $\mathbf{Q_A}$. Coefficient λ is applied to characterize the relationship between $\mathbf{Q_A}$ and E that $\mathbf{Q_A}= \lambda E$ ($\lambda \propto 1/(d_A C_A)$ and d_A is the distance between two accumulators). In this case, the density of the leakage current $j_{leakage}$ can be defined as following equation:

$$\mathrm{j}_{leakage} = \sigma_m \cdot e^{(\frac{Q_A}{Q_B})} \cdot Q_A \cdot \lambda = \sigma_m \cdot e^{(\frac{([Nnt])q}{60 \cdot Q_B})} \cdot Q_A \cdot \lambda \quad (5)$$

And the leakage current $i_{leakage}$ can be defined as following equation:

$$\mathrm{i}_{leakage} = \sigma_m \cdot e^{(\frac{([Nnt])q}{60 \cdot Q_B})} \cdot Q_A \cdot \lambda \cdot S_A \quad (6)$$

Taking the coefficient A as $\lambda\sigma_m S_A$, the charge leakage on accumulators ($\mathbf{Q_{leakage}}$) can be define as:

$$\mathrm{Q}_{leakage} = \int_0^t i_{leakage}\, dt = \int_0^t \left[\frac{Nnt}{60}\right] \cdot q \cdot Ae^{\left(\left[\frac{Nnt}{60}\right] \cdot \frac{q}{Q_B}\right)} dt \tag{7}$$

Reference

1. X. Chen *et al.*, Modeling a dielectric elastomer as driven by triboelectric nanogenerator. *Applied Physics Letters,* 2017, **110**, 033505.
2. C. Chiang Foo *et al.*, Model of dissipative dielectric elastomers. *J. Appl. Phys.,* 2012, **111**, 034102.

Supplementary Note S3. The calculation of energy conversion efficiency (η%).

The energy conversion efficiency (η%) can be estimated through the conversation of energy , which has been demonstrated by previous study [1]. η can be calculated based on the equation:

$$\eta\% = \frac{E_{ele}}{E_{input}} \times 100\%$$

, where E_{ele} is the electrical energy generated in one step, and E_{input} is the energy for operating the TENG. The maximum electrical energy (E_{ele}) generated by the SH-TENG in one step can be estimated using the output signal of the TENG with external load (Fig. 3e) and the highest power output is reached at the resistance of 10GΩ. It can be calculated according to the following equation: $E_{ele} = \int I^2 R dt$. Through the integration, we can get: E_{ele} =0.062mJ. The energy input for driving SH-TENG is divided into three parts: the electrostatic energy (E_{es}) of the two oppositely-charged dielectric materials (Kapton and Nylon), the electrical energy (E_{ele}) of the TENG generated on the pair of trans-electrodes when the disk moving 1 step, and the heat dissipated during mechanical sliding of dielectric materials and tribo-electrodes. As for the electrostatic energy E_{es}, it can be estimated as:

$$E_{es} = U_1 \sigma S + U_2(-\sigma)S = (U_1 - U_2)\sigma S,$$

where U1 and U2 are the potentials at the Kapton and Nylon, respectively; σis the charge density of the dielectric materials; and S is the area of the single transporting electrode. Here, we can do some approximate calculation. The charge density on the electrified trans-electrodes can be considered as the same as the charge density of the dielectric materials (σ).Thus, the potential difference of dielectric materials (U1-U2) can be replaced as that the potential difference of a pair of electrified trans-electrodes (Voc). So, the electrostatic energy E_{es} can be estimated as:

$$E_{es} = (U_1 - U_2)\sigma S = V_{oc} \times \sigma S = V_{oc} \times Q_{sc},$$

In this estimation, we assume the rotation speed of SH-TENG is 50rpm. From the electrical measurement of the TENG, V_{OC} is 15900V and Q_{SC} for TENG moving 1step is 19nC. Thus, we can get

$$E_{es} = V_{oc} \times Q_{sc} = 15900V \times 19 \times 10^{-9}C = 0.3021mJ$$

The other part of energy input is the heat dissipated during mechanical sliding, which is rather difficult to estimate for the current design. Considering that Kapton and Nylon are very smooth materials and the friction resistance is very small, we can ignore the component of heat dissipated. Thus, the energy input E_{input} can be estimated to be:

$E_{input} = E_{ele} + E_{es}$=0.3641mJ.

The maximum energy conversion efficiency can be estimated as follows:

$$\eta_{0/0} = \frac{E_{ele}}{E_{input}} \times 100\,{}^{0}/_{0} = 17.03\%$$

Reference

[1] S. Wang *et al.*, Sliding-Triboelectric Nanogenerators Based on In-PlaneCharge-Separation Mechanism. *Nano Lett.,* 2013, **13**, 2226-2233.

Supplementary Table S1.The list of possible choices for triboelectric materials

Negative electrified materials	Positive electrified materials
Kapton	Nylon
(Fluorinated-ethylene-propylene) FEP	Wool fabric
(Poly-tetra-fluoroethylene) PTFE	Silk fabric
(Polyvinyl-chloride) PVC	high-energy radiation treated Kapton [1]
(polydimethylsiloxane) PDMS	Oil-resistant buna-N rubber
(Polyethylene terephthalate) PET	
(polystyrene) PS	
(Polycarbonate) PC	
(polyethylene) PE	

Reference

[1] S. Li *et al.*, Manipulating the triboelectric surface charge density of polymers by low-energy helium ion irradiation/implantation. *Energy Environ. Sci.,* 2020, **13**, 896-907

Supplementary Table S2. Comparison with other high voltage TENG

article	sustainable	Voltage
Zhu.etal [*1*]	No	0.87KV
Chen.etal [*2*]	No	2.4KV
Nie.etal [*3*]	No	6KV
Xu.etal [*4*]	YES	7KV
Li.etal [*5*]	YES	8KV
Huo.etal [*6*]	YES	8KV
Wang.etal [*7*]	No	12KV
Wang.etal [*8*]	No	15KV
This work	Yes	>20KV

Reference

1. G. Zhu, J. Chen, T. Zhang, Q. Jing, Z. L. Wang, Radial-arrayed rotary electrification for high performance triboelectric generator. *Nat. Commun.* **5**, 3426 (2014).
2. X. Chen, T. Jiang, Y. Yao, L. Xu, Z. Zhao, Z. L. Wang, Stimulating Acrylic Elastomers by a Triboelectric Nanogenerator – Toward Self-Powered Electronic Skin and Artificial Muscle. *Adv. Funct. Mater.* **26**, 4906-4913 (2016).
3. J. Nie, Z. Ren, J. Shao, C. Deng, L. Xu, X. Chen, M. Li, Z. L. Wang, Self-powered microfluidic transport system based on triboelectric nanogenerator and electrowetting technique. *ACS Nano* **12**, 1491-1499 (2018).
4. L. Xu, H. Wu, G. Yao, L. Chen, X. Yang, B. Chen, X. Huang, W. Zhong, X. Chen, Z. Yin, Z. L. Wang, Giant Voltage Enhancement via Triboelectric Charge Supplement Channel for Self-Powered Electroadhesion. *ACS Nano* **12**, 10262-10271 (2018).
5. C. Li, Y. Yin, B. Wang, T. Zhou, J. Wang, J. Luo, W. Tang, R. Cao, Z. Yuan, N. Li, X. Du, C. Wang, S. Zhao, Y. Liu, Z. L. Wang, Self-Powered Electrospinning System Driven by a Triboelectric Nanogenerator. *ACS Nano* **11**, 10439-10445 (2017).
6. H. Huo, F. Liu, Y. Luo, Q. Gu, Y. Liu, Z. Wang, R. Chen, L. Ji, Y. Lu, R. Yao, Triboelectric nanogenerators for electro-assisted cell printing. *Nano Energy* **67**, 104150 (2020).
7. X. Wang, S. Niu, Y. Yin, F. Yi, Z. You, Z. L. Wang, Triboelectric Nanogenerator Based on

Fully Enclosed Rolling Spherical Structure for Harvesting Low-Frequency Water Wave Energy. *Adv. Energy Mater.* **5**, 1501467 (2015).

8. S. Wang, Y. Xie, S. Niu, L. Lin, Z. L. Wang, Freestanding Triboelectric-Layer-Based Nanogenerators for Harvesting Energy from a Moving Object or Human Motion in Contact and Non-contact Modes. *Adv. Mater.* **26**, 2818-2824 (2014).

Supplementary Table S3. Physical parameters of the LDPE, carbon, dimethylsilicone oil, FC-40 (Temperature 25°C)

Physical parameters	LDPE	carbon	dimethylsilicone oil	FC-40
Density(kg/m^3)	965	2260	963	1850
Relative permittivity	2.175	12	2.4	1.9
viscosity(N·s/m^2)	\	\	0.02889	0.0034
Diameter of particles (μm)	120	120	\	\